University of Groningen

Bacterial interactions with nanostructured surfaces

Hizal, Ferdi

IMPORTANT NOTE: You are advised to consult the publisher's version (publisher's PDF) if you wish to cite from it. Please check the document version below.

Document Version
Publisher's PDF, also known as Version of record

Publication date:
2017

Link to publication in University of Groningen/UMCG research database

Citation for published version (APA):
Hizal, F. (2017). *Bacterial interactions with nanostructured surfaces*. [Thesis fully internal (DIV), University of Groningen]. Rijksuniversiteit Groningen.

Copyright
Other than for strictly personal use, it is not permitted to download or to forward/distribute the text or part of it without the consent of the author(s) and/or copyright holder(s), unless the work is under an open content license (like Creative Commons).

The publication may also be distributed here under the terms of Article 25fa of the Dutch Copyright Act, indicated by the "Taverne" license. More information can be found on the University of Groningen website: https://www.rug.nl/library/open-access/self-archiving-pure/taverne-amendment.

Take-down policy
If you believe that this document breaches copyright please contact us providing details, and we will remove access to the work immediately and investigate your claim.

Downloaded from the University of Groningen/UMCG research database (Pure): http://www.rug.nl/research/portal. For technical reasons the number of authors shown on this cover page is limited to 10 maximum.

Download date: 05-05-2023

CHAPTER 2

Nanoengineered Superhydrophobic Surfaces of Aluminum with Extremely Low Bacterial Adhesivity

Published in ACS Applied Materials and Interfaces ***2017****, 9 (13), 12118-12129*

ABSTRACT

Bacterial adhesion and biofilm formation on surfaces are troublesome in many industrial processes. Here, nanoporous and nanopillared aluminum surfaces were engineered by anodizing and post-etching processes and made hydrophilic (using the inherent oxide layer) or hydrophobic (applying a Teflon coating) with the aim of discouraging bacterial adhesion. Adhesion of Staphylococcus aureus ATCC 12600 (Gram-positive, spherically-shaped) and Escherichia coli K-12 (Gram-negative, rod-shaped) was evaluated to the nanoengineered surfaces under both static and flow conditions (fluid shear rate of 37 s^{-1}). Compared to a non-structured electropolished flat surface, the nanostructured surfaces significantly reduced the number of adhering colony forming units (CFUs) for both species, as measured using agar plating. For the hydrophilic surfaces, this was attributed to a decreased contact area, reducing bacterial adhesion forces on nanoporous and nanopillared surfaces to 4 and 2 nN, respectively, from 8 nN on flat surfaces. Reductions in the numbers of adhering CFUs were more marked on hydrophobic surfaces under flow, amounting to more than 99.9 and 99.4% for S. aureus and E. coli on nanopillared surfaces, respectively. Scanning electron microscopy revealed the few bacteria found on the hydrophobic nanopillared surfaces adhered predominantly to defective or damaged areas, whereas the intact area preserving the original nanopillared morphology was virtually devoid of adhering bacteria. The greater decrease in bacterial adhesion to hydrophobic nanopillared surfaces than to hydrophilic or nanoporous ones is attributed to effective air entrapment in the three-dimensional pillar morphology, rendering them superhydrophobic and slippery, in addition to providing a minimized contact area for bacteria to adhere to.

INTRODUCTION

Bacterial adhesion and biofilm formation on surfaces are significant issues in many industrial processes, causing a decrease in efficiency and thus an increase in operating costs. Typical examples include medical implants and devices, food processing equipment, pipelines, water treatment plants, heat exchangers, and ship hulls.[1–3] In particular, microbial adhesion and biofilm formation can cause serious health hazards when on medical devices, implants, and food processing equipment. Metallic materials such as titanium, steel and aluminum are widely used in such applications and can additionally become subject to microbially induced corrosion.[4] In medical applications, mechanical removal of biofilms is considered a last resort solution, as compared to industrial applications which can more easily handle such an expensive yet effective approach. Some methods of treatment and prevention include antibiotics, however, with the increasing number of resistant strains and the desensitizing properties of biofilms, antibiotics are rendered highly ineffective now more than ever before.[5] Antibacterial coatings have also been explored to prevent biofilm formation to combat the increasing problems associated.[6–9] Cationic, quaternary ammonium coatings killing adhering bacteria on contact, provide one way to prevent biofilm formation.[10] Coatings can also work as a reservoir for antibiotics housing, but not seldom tend to have released their antibiotic content when infection occurs.[11,12] Polymer brush coatings are directly repelling bacteria, but do attract weakly adhering biofilms.[13]

A different approach explored in the prevention of bacterial adhesion and biofilm formation is to mechanically or chemically engineer surface properties, such as roughness and hydrophobicity. The nature of the adhesion forces plays a key role in mediating interactions in bacterial adhesion to surfaces,[14] although no general conclusions have been drawn with respect to effects of roughness and hydrophobicity on bacterial adhesion to surfaces valid for different strains and species and under different environmental conditions due to the multifactorial nature of bacterial adhesion and biofilm formation in particular.[15] Recently, the importance of the effects of nanoscale features have also been reported,[16,17] as summarized in Table 1.[18–30] Adhesion of staphylococci was notably reduced on pillar-patterned poly(ethylene glycol) hydrogels when the spacing between the structures was 1.5 μm or less.[21] This suggests that the critical length scale of surface features for effective prevention of bacterial adhesion should be nanoscale (i.e. smaller than the size of a bacterium).[21] Nanopillared structures of silicon effectively killed bacteria due to high mechanical pressures locally exerted on the bacterial cell membrane in Pseudomonas aeruginosa ATCC 9027, Staphylococcus aureus 65.8^T, and spores of Bacillus subtilis NCIMB 3610^T.[22] Moreover, the effective physical contact area of adhering bacteria on a nanostructured surface is likely to be less than on a non-structured one, resulting in weaker overall adhesion forces,[23] which may result in suppression of the activation of bacterial antibiotic-defense mechanisms.[31] Whereas randomly-roughened titanium alloy surfaces increased bacterial adhesion due to enlarged bacterial-surface contact area,[28] titanium oxide (TiO_2) nanotube surfaces showed reduced bacterial adhesion, growth, and viability due to the unique properties found in titanium, including titanium crystallinity,

modified surface chemistry, and photocatalytic activity.[25,29] Gentamicin-loaded titanium oxide nanotubes have also been used to decrease bacterial growth.[24] Nanostructures of titanium oxide also showed enhanced antibacterial efficacy of antibiotic coating due to the increase in the effective surface area for drug loading and the decrease in the bacterial adhesion force.[27] The combined effects of surface nanostructures and hydrophobicity were also demonstrated using well-regulated nanostructures with relatively high aspect ratios on softwood fiber,[18] polyurethane,[16] and titanium,[26] making the surface superhydrophobic with the entrapment of air in the textured structures, which led to reduce bacterial contact with the material and therewith adhesion. However, such effects were not significant when the surface nanostructures were not well defined to have relatively high aspect ratios, which could not lead to the entrapment of the air in the textured surfaces, as demonstrated on stainless steel.[30] Immobilized liquid (e.g. oil) within hydrophobic nanoporous surfaces also prevented bacterial attachment due to lubrication effects of the liquid layer.[20]

Although various materials have been engineered and explored for the fundamental studies and applications for the reduction of bacterial adhesion and biofilm formation by exploiting the effects of surface nanostructures and hydrophobicity, the possible merits of nanostructured surfaces combined with the modulation of surface hydrophobicity have not yet been systematically explored, especially not for aluminum, which is one of the most practical materials for many engineering devices and systems, for different bacterial strains and in absence or presence of fluid flow, as highlighted in Table 1. Therefore, the main objective of this study is to develop well-regulated nanostructured surfaces on aluminum substrates and to evaluate their merits with respect to preventing adhesion of S. aureus (Gram-positive, spherically-shaped) and Escherichia coli (Gram-negative, rod-shaped) on novel three-dimensional (3D) nanopillared surfaces compared to conventional two-dimensional (2D) nanoporous ones, both conditioned to be either hydrophilic or hydrophobic and subjected to bacterial adhesion under static and flow conditions. The novel 3D nanopillared surfaces of aluminum are nanoengineered by modulating anodizing and post-etching processes. Electrochemical anodizing is a cost-effective and scalable technique to create nanostructures of metallic substrates with arbitrary curvatures over a large surface area with independent controllability of their three-dimensionality,[32] which is a major advantage in real applications. S. aureus and E. coli were chosen for this study because they are potentially pathogenic strains involved in several types of human infection and foodborne illnesses.[33] Numbers of viable bacteria adhering to the different surfaces prepared are enumerated from the number of colony forming units (CFUs) after dispersal of adhering bacteria and agar plating. Scanning electron microscopy (SEM) and atomic force microscopy (AFM) are further employed to visualize the bacterial adhesion on the surfaces and also estimate single-bacterial adhesion forces on the surfaces, respectively.

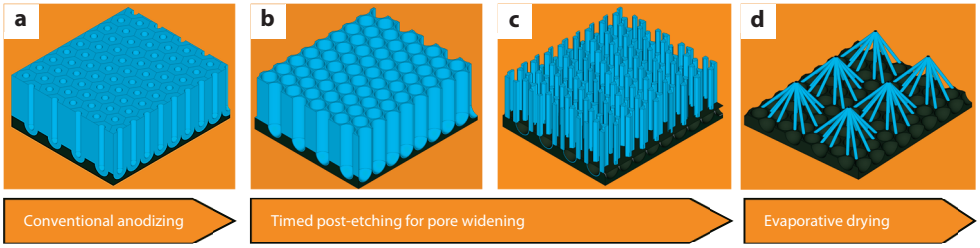

Figure 1. *Schematic of the fabrication process to transform nanoporous structures of anodic aluminum oxide (AAO) to nanopillar structures. (a) Initial nanoporous AAO pattern. (b) Nanoporous AAO pattern with enlarged pore size by pore-widening (post-etching) process. (c) Nanopillar AAO pattern with further etching, resulting in the formation of disconnected individual pillar nanostructures. (d) Nanopillar AAO pattern with evaporative drying, resulting in the aggregation of the individual pillar structures and hence the formation of the clustered pillar (or conical) structures due to capillary force.*

FABRICATION SCHEME

Figure 1 shows the schematics of the fabrication processes of novel 3D nanopillared surfaces from conventional 2D (planar) nanoporous surfaces of aluminum employing anodizing, post-etching, and evaporative drying processes successively. Initially, an electropolished aluminum substrate is conventionally anodized in an aqueous acidic solution, resulting in the formation of a self-ordered 2D nanoporous alumina layer (Figure 1a). The following chemical etching process widens the pores, making the walls between the two adjacent pores thinner (Figure 1b). With the elongated pore-widening, high-aspect-ratio 3D pillared alumina nanostructures are formed by the thinned walls, protruding from the barrier layer (Figure 1c). When the pillared surface is dried during evaporation after the wet anodizing and post-etching processes, clustered pillar structures of a conical shape are formed due to the capillary force during the evaporative drying process, which is referred to as a nanocarpet effect[34,35] (Figure 1d).

Hard anodizing techniques were previously reported to achieve similar nanopillared surfaces of aluminum, using impulsive high anodizing voltages.[32] High shear forces were also employed based on the so-called bamboo-splitting model to engineer similar nanopillared surfaces of titanium by stirring anodizing solution intensively at high rate during anodizing process.[27] Such methods are one-step fabrication processes, not requiring the additional post-etching process employed in this study. However, in such methods, the regulation and the determination of the proper anodizing voltages or stirring intensities/rates as well as the anodizing time to result in the formation of the well-defined pillared morphology remain a challenge. The uniformity of the patterned nanostructures over the entire surface area is another concern. In contrast, the post-etching technique employed in this study allows us to have more control and uniformity on the dimensions and shapes of the nanostructures and more flexibility in the transformation from the conventional 2D nanoporous morphology to the 3D nanopillared one than the other methods.

MATERIALS AND METHODS

Fabrication of Nanoporous and Nanopillared Surfaces of Aluminum. Aluminum foils (0.5 mm thickness, 99.98 % purity, Alfa Aesar, Ward Hill, MA, USA) were cut into 1 cm × 1 cm specimens and then degreased in metal cleaner solution (MC-3, Branson, Danbury, CT, USA), acetone and ethanol (100%) using an ultrasonic cleaner for 10 min and subsequently rinsed in deionized water and dried by N_2 gas. Aluminum foils were then electropolished in a solution of perchloric acid and ethanol ($HClO_4/C_2H_5OH$ = 1:4 in volumetric ratio) under an applied potential of 20 V for 2 min to remove surface irregularities.

In order to fabricate a nanoporous aluminum surface (Figure 1a), electropolished specimens were submerged in 0.3 M oxalic acid ($C_2H_2O_4$) solution which was placed in a double-walled glass beaker at 7°C and anodized for 15 min at 45 V using a DC power supply (Genesys 300-17, TDK-Lambda, NJ, USA). The aluminum foil was used as a working electrode (anode), and a platinum foil was employed as a counter electrode (cathode) in the anodizing process. The two electrodes were separated at a distance of 5 cm. During the electrochemical process, the solution was stirred at 150 rpm using a magnetic stirrer to help maintain constant temperature and uniform anodization over the sample surface. After the anodizing process, each specimen was kept in ethanol for 10 min and carefully rinsed in deionized water to remove the residue of the electrolytic solution.

In order to fabricate a nanopillared aluminum surface (Figure 1c), the nanoporous surface specimens were etched in 5% wt. phosphoric acid (H_3PO_4) at 30°C for regulated periods. Whereas relatively short etching periods (e.g. up to around 50 min) still result in the 2D nanoporous surface with an enlarged pore size during the pore-widening process (Figure 1b), elongated etching thins down the pore walls and eventually leaves individual (disconnected) pillared nanostructures (Figure 1c). Finally, the specimens were gently dried by evaporation with nitrogen gas. During the evaporation, the individual nanopillared structures get amalgamated to form clustered nanopillars of a conical shape due to the capillary force (Figure 1d). Such a structural transformation during the evaporation results in the change in color of the sample surface. Typically, a light purplish reflection is observed from the surface when the individual singular nanopillar structures form the array of amalgamated conical pillared clusters.

The structural morphology of the fabricated surfaces was characterized by using field-emission scanning electron microscopy (FE-SEM, Quanta FEG450, FEI, Hillsboro, Oregon 97124 USA).

Creation of a Hydrophilic or Hydrophobic Surface. For a hydrophilic surface condition of the nanoporous and nanopillared surface samples, the inherent hydrophilicity of the anodic aluminum oxide surface was used.

For a hydrophobic surface, the fabricated surfaces were coated with Teflon. Before Teflon coating, samples were cleaned in O_2 plasma (PDC-001, Harrick Plasma Inc., NY, USA) for 15 min to remove organic residues. Then, samples were spin-coated with 0.2 wt % Teflon solution

(a mixture of Teflon AF1600 powder (DuPont) and perfluoro-compound FC-75 (Fisher Scientific)) at 1000 rpm with a ramp of 500 rpm in 30 s which resulted in a film thickness of a couple of nanometers. Each sample was baked on a hot plate at 110°C for 10 min to evaporate the solvent and baked again at 165°C for 5 min and at 330°C for 15 min to improve adhesion. Finally, the samples were rinsed by 2-propanol and deionized water for 5 min and dried in air for 1 day before measuring water contact angles.

For water contact angle measurements, the contact angle of a sessile droplet (about 3 μl) of deionized water was measured on each sample at room temperature by using a contact angle goniometer (Model 500, Ramé-hart). Contact angles were measured on more than five different places over each surface sample to obtain average values.

Bacterial Adhesion. S. aureus ATCC 12600 and E. coli K-12 were separately grown in tryptic soy broth (TSB) at 37°C for 24 h. Thereafter, bacteria were suspended in 100 mM phosphate buffer saline (0.27 mM potassium chloride, 13.7 mM sodium chloride, 100 mM potassium phosphate) at a pH of 7.5. The initial concentrations of bacteria in phosphate buffer, as enumerated by agar plate counting, were 3×10^8 CFU per ml. Bacterial adhesion was carried out on three 1×1 cm^2 samples at the same time, including flat, nanoporous, and nanopillared surface samples placed together side-by-side inside a parallel-plate flow channel (see Figure S1). Hydrophilic and hydrophobic samples were evaluated separately. The top and bottom chamber plates of the parallel-plate flow channel were sonicated for 3 min in 2% RBS 35 (Thermo Fisher Scientific, Waltham, MA, USA) followed by rinsing with tap water, deionized water, methanol, tap water, and finally deionized water. For adhesion under static conditions, bacterial suspensions were simply held inside the pre-cleaned test chamber containing the three different types of test samples. For adhesion under flow, bacterial suspensions (viscosity: around 5 mPa·s) were perfused through the chamber at a flow rate of 200 ml/min (average velocity: 1.33 cm/s, Reynolds number: around 10). The shear rate ($\dot{\gamma}$, s^{-1}) at the substrate surface (i.e. channel wall) in the parallel-plate rectangular channel was 37 s^{-1}, estimated by the Hagen–Poiseuille equation:

$$\dot{\gamma} = \frac{3Q}{2(h_0/2)^2 w_0} \tag{1}$$

where Q is the volumetric flow rate of the bacterial suspension, h_o and w_o are height (3.3 mm) and width (50 mm) of the parallel-plate rectangular channel. Both static and flow experiments were run for 1 h and carried out in triplicate with separately prepared samples and different bacterial cultures. Non-adhering bacteria were removed from the flow chamber by flowing 10 ml of sterile buffer solution at the same flow rate.

Bacterial Adhesion Numbers. In order to count the number of the bacteria adhering to the surfaces, the bacteria were removed from the surfaces using sonication, as a slight modification of the method reported by Zhao et al. (2008)[36]. Each specimen was placed in a sterile beaker containing 10 ml of 0.1% sterile peptone water and subsequently put in an

ultrasonic bath and sonicated for 10 min at a temperature not exceeding 25°C. Thereafter, 100 µl of resulting suspension was serially diluted (10^{-1}, 10^{-2}, and 10^{-3}) and dilutions were agar-plated in triplicate, and incubated overnight at 37°C. The number of CFUs on the plates was counted and expressed per cm^2 substrate surface area. The total numbers of adhering CFUs on the different surfaces were compared using a two-tailed Student's t-test. Differences were considered significant if $p < 0.05$.

Electron Microscopy. For the electron microscopic imaging of adhering bacteria on the surfaces, specimens were taken out from the parallel-plate rectangular channel, rinsed with phosphate buffer and then moved into a six-well plate without exposing the specimens to an air-liquid interface. 2% glutaraldehyde was added and samples were kept in a refrigerator at 4°C overnight for fixation. Afterwards, the surfaces were washed with 0.1 M cacodylate buffer, followed by 1 h of incubation at room temperature with 1% OsO_4 in 0.1 M cacodylate buffer, washed with deionized water and dehydrated with 30, 50, 70% ethanol for 15 min each and three times with absolute ethanol for 30 min at 4°C. Finally, the samples were incubated in ethanol (100%) and tetramethylsilane (1:1) for 10 min, followed by 15 min incubation in pure tetramethylsilane and air-drying. Samples were kept wet in the associated solutions throughout the fixation process until the last air-drying step. FE-SEM was used to visualize the adhering bacteria.

Bacterial Adhesion Forces. Bacterial adhesion forces on the samples were measured using atomic force microscopy (AFM, BioScope Catalyst, Bruker, CA, USA) with ScanAsyst (Veeco Instruments Inc., CA, USA). Before each measurement, cantilevers were calibrated by the thermal tuning method,[37] yielding an overall average spring constant of 0.042 ± 0.003 N/m. Single-bacterial contact probes were prepared by immobilizing single bacteria on an NP-O10 (Bruker AFM Probes, Camarillo, CA) tipless cantilever through electrostatic attraction. All adhesion force measurements were performed in phosphate buffer at room temperature with z-scan rates of 1.0 Hz under a loading force of 5 nN at five randomly chosen spots (ten force curves per spot) over a sample surface.

RESULTS AND DISCUSSION

Figure 2 shows the FE-SEM images of the nanostructured alumina surfaces (before Teflon coating) fabricated on aluminum substrates according to the scheme illustrated in Figure 1. Figure 2a shows the hexagonal array of self-ordered nanopores of the alumina layer that was formed with a conventional anodization process in 0.3 M oxalic acid electrolyte at 45 V and 15°C. The pore diameters and the interpore distances are affected by the anodizing voltage and temperature at the given electrolyte type and concentration.[38,39] Based on the FE-SEM images, the average pore size and the interpore distance of the nanopore structures fabricated with anodizing (Figure 2a) were measured to be 28 ± 2 nm and 50 ± 3 nm, respectively.

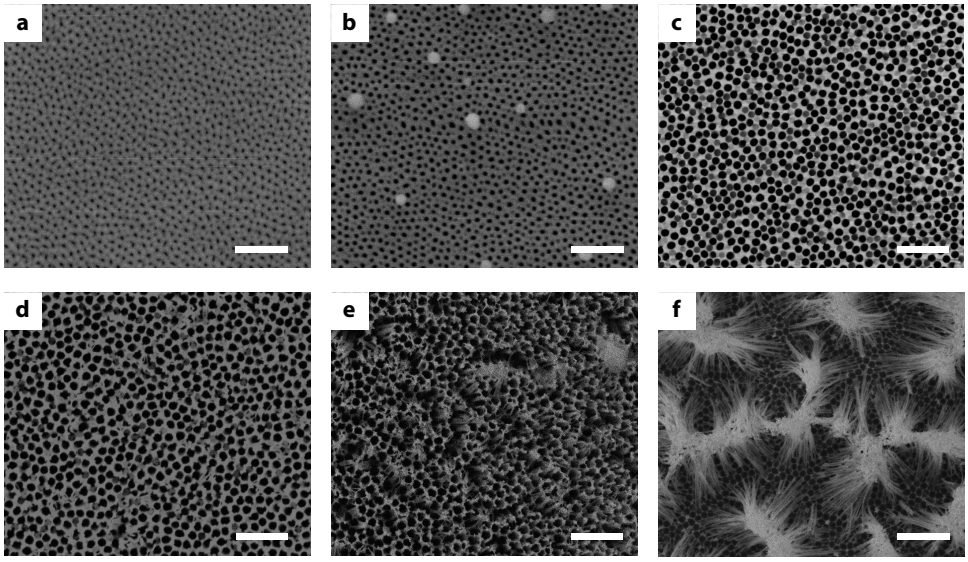

Figure 2. *Field emission scanning electron microscopy (FE-SEM) images of nanostructured alumina surfaces by anodizing, also followed by post-etching in 5% wt phosphoric acid (H_3PO_4) at 30°C. (a) As anodized, (b) Post-etching in 15 min, (c) Post-etching in 25 min, (d) Post-etching in 35 min, (e) Post-etching in 45 min, (f) Post-etching in 55 min. Scale bar in each image indicates 500 nm.*

Meanwhile, the duration of anodizing influences the thickness of the porous oxide layer. The growth rate of the oxide layer in the anodizing condition applied was measured to be 1.6 nm/s. Based on the growth rate, the anodization was applied for 15 min to form high-aspect-ratio nanoporous structures of the alumina layer of around 1.5 μm in thickness. Figures 2b-2f show the transformation of the nanostructural morphology from nanoporous to nanopillared, regulated by the duration of post-etching. In particular, Figure 2f shows the self-aggregated nanopillars of the alumina layer, as illustrated in Figure 1d. Individual alumina nanopillars were first formed near the triple points of the intersected hexagonal pores with the regulated pore-widening process in post-etching. The etching rate during the pore-widening process was calculated from the FE-SEM images of the surface patterns and found to be 0.7 nm/min, which required 55 min to achieve individually standing pillars. The high-aspect-ratio single-pillar nanostructures were then inclined and aggregated during a drying process due to the capillary force among the nanostructures, resulting in the self-formation of the clustered nanopillar structures in a cone shape in air.[32] The average distance between the clustered conical pillars amounted to around 1 μm with a height of the clustered pillars of around 1 μm and a sidewall angle of around 60°. In this study, the nanoporous surface (Figure 2a) and the nanopillared surface with the post-etching for 55 min (Figure 2f) were used for hydrophilic nanostructured surfaces. The hydrophobic nanostructured surfaces were coated with Teflon, as shown in Figure 3. The thickness of the Teflon coating was not more than a couple of nanometers (Figure S2), regulated by the concentration of the Teflon solution and the spin coating speed, and therewith did not affect the integrity and dimensions of the surface nanostructures.[41]

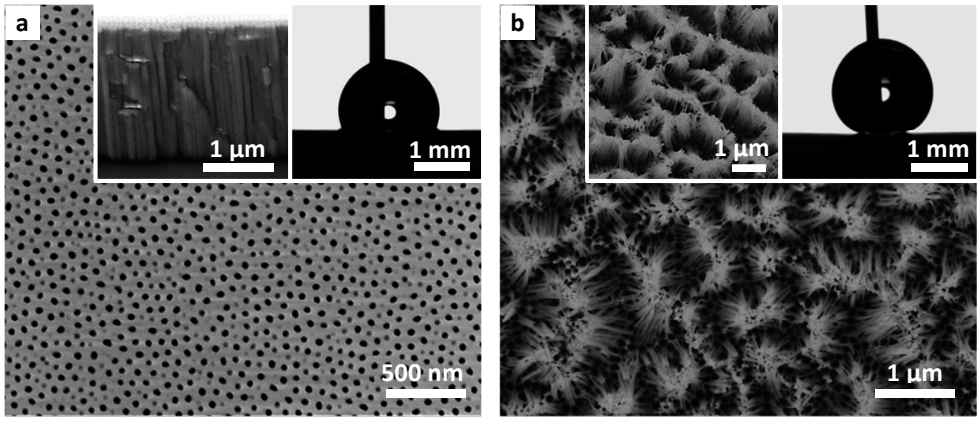

Figure 3. *FE-SEM images of Teflon-coated hydrophobic nanostructured alumina layers on aluminum substrates. (a) Nanoporous and (b) Nanopillared AAO. The top left inset in each figure shows the cross-sectional (a) or tilted view (b) of the fabricated nanostructures. The top right inset in each figure shows a sessile droplet of deionized water on each surface yielding contact angles of 115° and 162°, respectively.*

The contact angle of a sessile droplet of deionized water measured on the inherent (i.e., before Teflon coating) nanoporous surfaces (Figure 2a) was 17 ± 7°, while on the inherent nanopillared surfaces (Figure 2f) full spreading was observed (0° contact angle). The contact angle on the flat electropolished aluminum surface before anodizing (but with a thin native oxide layer) was 70 ± 3°. Thus the nanostructures make an inherently hydrophilic surface even more hydrophilic, which is more pronounced with 3D nanopillar structures than 2D nanopore structures in agreement with the Wenzel equation.[40] On the other hand, the contact angle on a Teflon-coated flat aluminum surface amounted to 110 ± 3° and increased upon Teflon-coating of nanoporous and nanopillared surfaces to 115 ± 2° and 162 ± 4°, respectively (insets to Figure 3a and Figure 3b). Accordingly, the nanostructures make the hydrophobized surface even more hydrophobic, especially for the high-aspect-ratio 3D nanopillared surface. The increase in water contact angle implies the entrapment of air between the liquid water and the nanostructured solid surface, which makes the liquid have a partial contact to the top solid surface of the AAO nanostructures, in line with the Cassie-Baxter model.[42] According to the Cassie-Baxter model,[42] the wetted solid area fraction over the projected surface area for the hydrophobized nanoporous and nanopillared surfaces are 0.88 and 0.07, respectively. The apparent contact angle of a water droplet on the 2D nanoporous surface increased only by around 5°, which is due to the small reduction of the wetted solid area fraction (by around 12% reduction). In contrast, the more significant increase of the contact angle on the 3D nanopillared surface (by around 52° increase) than the 2D nanoporous is due to the significant reduction of the wetted solid area fraction (by around 93% reduction) by the unique, pointed conical morphology of the clustered nanopillar structures that can maximize the entrapment of the air layer within the nanostructured surface. Such a decrease of the

wetted area of the hydrophobic surfaces, especially the 3D nanopillared surface, can be expected to minimize bacterial interactions with the surfaces.

Figure 4 shows the numbers of CFUs adhering to the different samples under different flow conditions, indicating a reducing trend in the CFUs for both *S. aureus* and *E. coli* as the surface topography changes from flat to nanoporous to nanopillared. This trend becomes more pronounced in the hydrophobic surface condition and under flow.

Particularly, Figure 4a and 4b show the bacterial adhesion numbers under static conditions for *S. aureus* and *E. coli*, respectively. On a hydrophilic surface, the 2D nanoporous surface showed negligible reduction in *S. aureus* and *E. coli* CFUs, compared to the flat aluminum surface. In contrast, on nanopillared surfaces, *S. aureus* and *E. coli* CFUs are significantly reduced (88% and 92%, respectively, as compared to a flat surface). At a given same surface topography, Teflon-coating significantly reduced the number of adhering CFUs for both strains, as compared to the corresponding hydrophilic surface condition. This effect was more pronounced on the nanostructured surfaces, especially on 3D nanopillared surfaces: i.e. for *S. aureus* 52, 80, and 85% for flat, nanoporous, and nanopillared surfaces, respectively, and for *E. coli* 66, 77, and 88% for flat, nanoporous, and nanopillared surfaces, respectively. In the hydrophobic surface condition, both 2D nanoporous and 3D nanopillared surfaces showed significant reductions in adhering CFUs as compared to the flat surface, again more pronounced on the 3D nanopillared surfaces (i.e. for *S. aureus* 62 and 96% for nanoporous and nanopillared surfaces, respectively, and for *E. coli* 58 and 97% for nanoporous and nanopillared surfaces, respectively). Compared to a hydrophilic flat surface, the hydrophobic nanopillared surface showed the most significant reduction in bacterial adhesion under static conditions (i.e. 98 and 99% for *S. aureus* and *E. coli*, respectively). For the given surface structure, the reduction in the number of adhering CFUs on the hydrophobic surface compared to the hydrophilic surface is partly due to the weakly polarizable Teflon layer which would reduce the Van der Waals interactions between bacteria and solid surfaces.[43] Meanwhile, on the nanostructured surfaces, the reduction of the bacterial adhesion is more significant due to the reduced effective solid surface area caused by entrapment of air in the nanostructured surfaces. This effect is more dramatic on the 3D nanopillared surface than the 2D nanoporous surface due to the more significant reduction of the solid area fraction wetted by the bacterial suspension on the 3D nanopillared surface. Moreover, the disconnected pillared morphology of the 3D nanopillared surface allows the air to exist as a continuous barrier layer under the liquid meniscus so that the bacteria would have the limited contact with the solid surface only by the isolated pointed tip. In contrast, the 2D nanoporous surface has continuous morphology for the solid surface so that the air would exist as localized cavity confined only within the disconnected pores and the bacteria can still have continuous and greater contact to the solid surface for the effective adhesion.

Figure 4c and 4d show bacterial adhesion under flow at a wall shear rate of 37 s^{-1} for *S. aureus* and *E. coli*, respectively. The effects of the surface nanotopography and hydrophobicity on the reduction in the numbers of adhering CFUs were more pronounced in

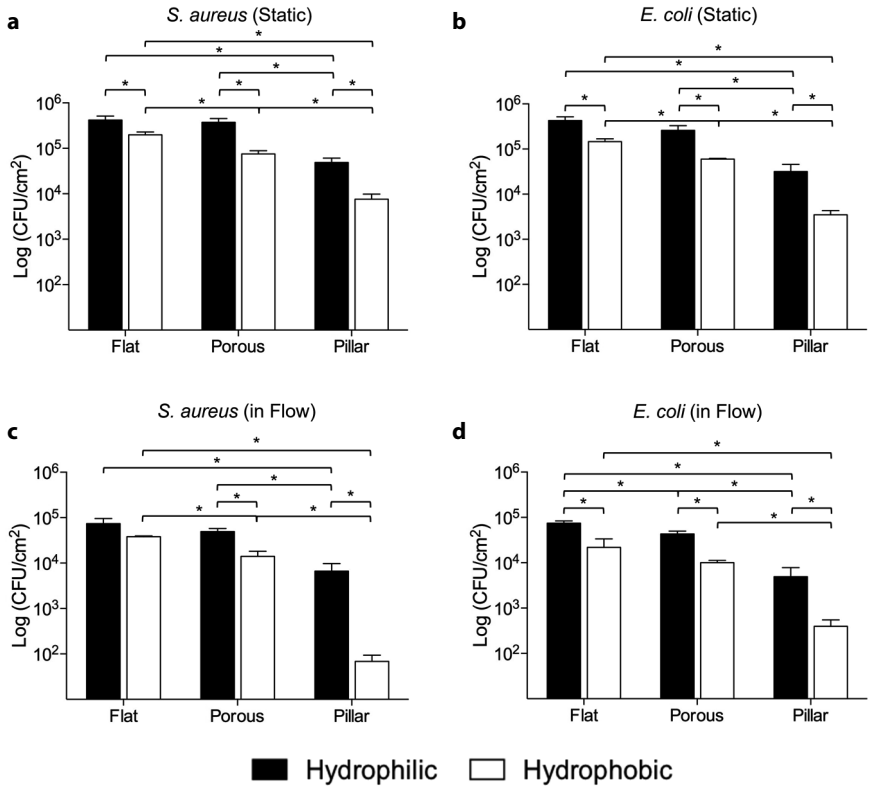

Figure 4. *Bacterial adhesion. The number of CFUs adhering to sample surfaces with different nanotopography (electropolished-flat, 2D-nanoporous, and 3D-nanopillared) and surface hydrophobicity under static (a and b) and flow (c and d) conditions (S. aureus, a and c; E. coli, b and d). Asterisks indicate statistical significance ($p < 0.05$ in a two-tailed Student's t-test) between indicated groups.*

the presence of flow than in its absence. Especially, the reductions under flow were most significant on hydrophobic nanopillared surfaces and larger in case of *S. aureus* (Gram-positive, spherically-shaped) than in case of *E. coli* (Gram-negative, rod-shaped). Compared to a hydrophilic flat surface, the reductions in CFUs on the hydrophobic nanopillared surface under flow were 99.9 and 99.4% for *S. aureus* and *E. coli*, respectively. Fluid shear can lead to the detachment of bacteria by sliding and rolling over a substrate surface.[44] According to the Stokes' law, the hydrodynamic force applied onto a spherical object in a low Reynolds number flow is proportional to the flow velocity that the object encounters with. On the hydrophobic nanopillared surface, adhering bacteria will experience a higher flow velocity than on a flat surface, due to effective slip flow at the interface between entrapped air and the liquid environment,[45] and hence the higher hydrodynamic detachment force. In contrast, the pore size and the interpore distance of the 2D nanoporous surface engineered by the conventional anodizing process are much smaller than the micron-sized bacteria. Therefore, water on hydrophilic surfaces or air retained in hydrophobic nanopores is

ineffective to develop an interface with discontinuous phase between the bacteria and the material so that the 2D nanoporous surface eventually allows significant bacteria-material interaction to enforce adhesion. Moreover, the effective slip flow on such 2D nanoporous hydrophobic surfaces is not so significant as on 3D nanopillared surface mainly due to the discontinuous arrangement of the air-liquid slip interface,[45] so that shear-induced detachment of adhering bacteria is not so effective on the 2D nanoporous surface.

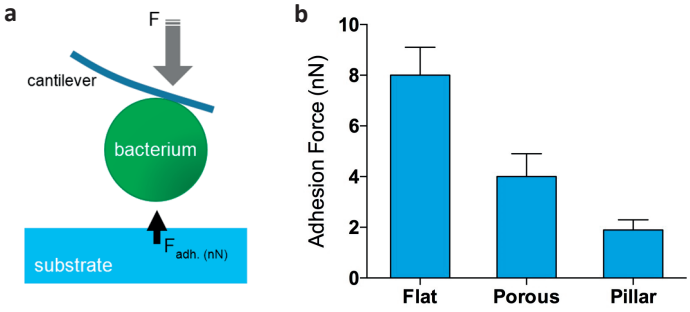

Figure 5. *Bacterial adhesion forces. (a) Scheme of single-bacterial contact probe atomic force microscopy with an immobilized bacterium attached on a tipless cantilever applied to measure bacterial adhesion forces. (b) S. aureus adhesion forces on hydrophilic flat, nanoporous, and nanopillared AAO surfaces. Five measurements were taken on random locations on each surface using a single bacterial probe under an applied normal force of 5 nN in phosphate buffer at pH 7.5 and room temperature.*

In this study, we used CFUs for enumeration, because in many applications the presence of CFUs is more relevant than the presence of dead bacteria that are non-culturable. While we cannot conclude whether the effects on the number of adhering CFUs are due to lower adhesion, detachment or killing of adhering bacteria, the effects of nanostructures on bacterial adhesion,[46] detachment and enhanced killing of adhering bacteria due to high local pressures on the bacterial cell wall[23,47] are likely to operate in concert to create the extremely low numbers of CFUs adhering to our superhydrophobically nanostructured aluminum surfaces.

Figure 5 confirms for a spherically-shaped *S. aureus* on hydrophilic surfaces that adhesion forces are lowest (2 ± 1 nN) on the nanopillared surface, compared to those on a flat (8 ± 2 nN) and nanoporous surfaces (4 ± 1 nN). This is mainly attributed to the small surface area effectively available for the bacterial adhesion on the 3D nanopillared surfaces compared to on the 2D flat or nanoporous surfaces. The lower adhesion force will more readily facilitate detachment of adhering bacteria from the hydrophobic nanopillared surface under flow than from the other surfaces. Note that bacterial adhesion forces for the rod-shaped organisms were not measured as the *E. coli* can adhere to the material surface either side-on or end-on making interpretation difficult. Also, air entrapment in the case of hydrophobic surfaces hampered reliable force measurements. However, effects of the reduced contact area demonstrated here for a spherically-shaped organism on hydrophilic surfaces will be equally valid for rod-shaped organisms and hydrophobic surfaces.

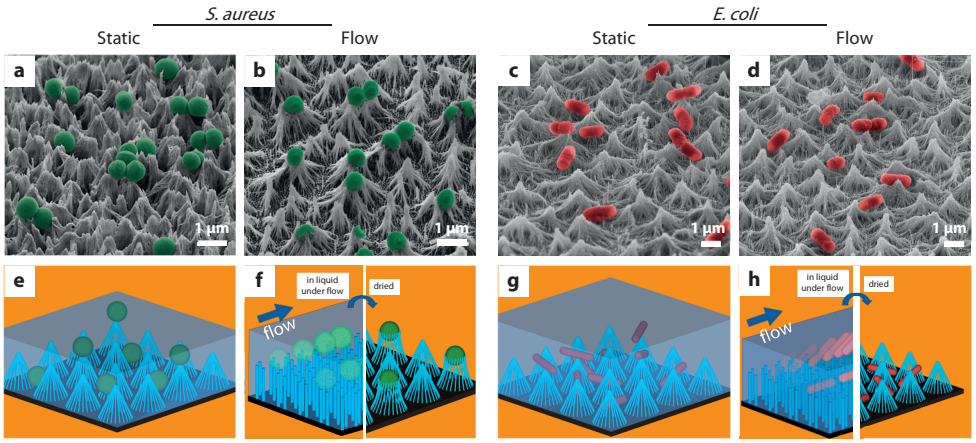

Figure 6. *FE-SEM images (a-d) and schematics (e-h) representing bacterial adhesion on hydrophilic nanopillared surfaces. S. aureus and E. coli are represented in artificially added green and red colors, respectively. In panels e and g, the schematics illustrate that the bacteria under static conditions adhere both at the nanopillar tips and in the valleys. In panels f and h, the left schematics represent unbundled nanopillars and drifting bacteria on them due to flow, whereas the right ones represent retained bacteria after the nanopillars get re-bundled during air-drying.*

To investigate the morphology of bacterial adhesion on the nanostructured surfaces, FE-SEM images were also taken after adhesion. Particularly, Figure 6 shows the FE-SEM images and the corresponding schematics of the adhesion of *S. aureus* and *E. coli* on the hydrophilic nanopillared surfaces. Under a static condition, the FE-SEM image (Figure 6a) shows that *S. aureus* adhere at the tips as well as in the valleys of the conically aggregated nanopillar structures, as illustrated in Figure 6e. The clustered conical surface morphology with periodicity similar to the bacterial dimensions and the hydrophilicity of the surface allow the bacterial suspension to wet the structured surface completely, increasing bacterial options to adhere. In contrast, under flow, *S. aureus* adhere mostly on the tips but little in the valleys and sometimes get trapped within nanopillared bundles (Figure 6b). As illustrated in Figure 6f, this is attributed to the effect of flow and drying artefacts due to SEM sample preparation. Under flow, fluid shear will disrupt the clustered nanopillars and unbundle them. The periodicity of the unbundled individual nanopillar structures is much smaller than the bacterial dimensions so that the bacteria adhere only on the tips of the nanostructures. When the surface dries in air for FE-SEM preparation, isolated nanopillars will get bundled back again to form the aggregated conical structures due to the capillary effect, causing the bacteria surrounded by the nanopillars. *E. coli* under static conditions (Figure 6c) show a similar behavior as *S. aureus*, adhering at the nanopillar tips as well as in the valleys (Figure 6g). However, unlike *S. aureus*, *E. coli* adhesion under flow (Figure 6d) occurs mostly in valleys and no *E. coli* appear to be surrounded by nanopillars. This is attributed to the anisotropic (rod-shaped) bacterial morphology of *E. coli*, which would make *E. coli* unstable and susceptible to fall or roll down to the valleys when the unbundled nanopillars get bundled back in drying (Figure 6h).

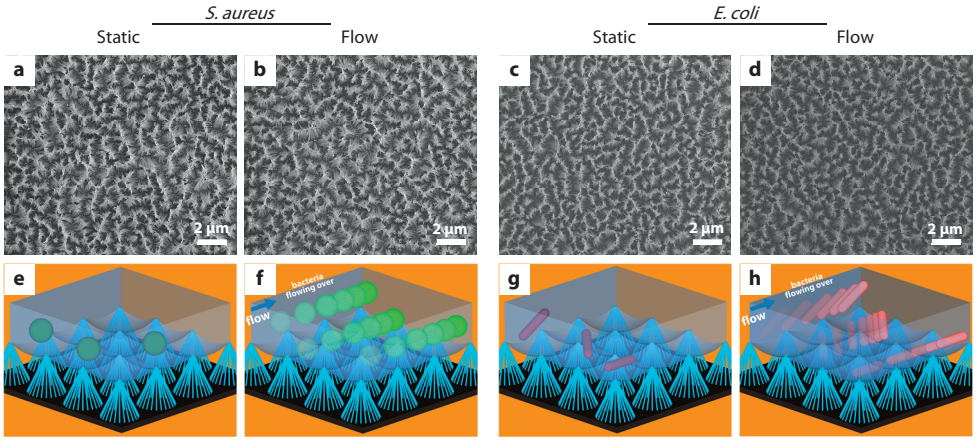

Figure 7. *FE-SEM images (a-d) and schematics (e-h) representing the bacterial adhesion on hydrophobic nanopillared surfaces. In panels e and g, the schematics represent the bacteria are floating over the entrapped air layer under a static condition. In panels f and h, the schematics represent the bacteria are driven off under flow.*

Figure 7 shows the FE-SEM images and the corresponding schematics of the bacterial adhesion on the hydrophobic nanopillared surfaces. The SEM images (Figure 7a-d) show that there are virtually no bacteria adhering on the surfaces regardless of the bacteria types and the flow conditions. This is attributed to the superhydrophobicity of the hydrophobized nanopillared surfaces, where the high fraction of retained air (Cassie-Baxter state)[42] minimizes the contact of bacterial suspension to the solid surface and hence bacterial adhesion, which is effective in both the static and flow conditions regardless of the bacterial strain involved. Under a static condition (as illustrated in Figure 7e and 7g) bacteria may adhere to the structural tips exposed to the liquid suspension. However, the bacteria were easily washed off by the buffer flow applied in rinsing, leaving the virtually bacteria-free surfaces (Figure 7a and 7c). It suggests that under flow, bacteria should get directly driven away with the regulated fluid shear as illustrated in Figure 7f and 7h, leaving the surfaces devoid of adhering bacteria (Figure 7b and 7d) even before the rinsing process. The hydrophobic nanopillared surfaces maintained the Cassie-Baxter state (air entrapment on the surface)[42] and did not allow the bacterial suspension to wet them throughout the adhesion assay under both static and flow conditions. The lubricating air layer entrapped at the interface between the bacterial suspension and the hydrophobic nanopillar structures helps the floating bacteria at the free surface to be driven off by the hydrodynamic force more easily, compared to the case of the hydrophilic nanopillared surfaces, due to the superhydrophobic slip effect.[45] Moreover, as opposed to the case of hydrophilic nanopillared surfaces, the hydrodynamic force does not reach the bundled nanopillar structures due to the interlayer of the air so that the unbundling effect of the conically clustered nanopillared structures by the hydrodynamic force as well as the re-bundling effect by the capillary force in drying in air are not present in the case of hydrophobic nanopillared surfaces.

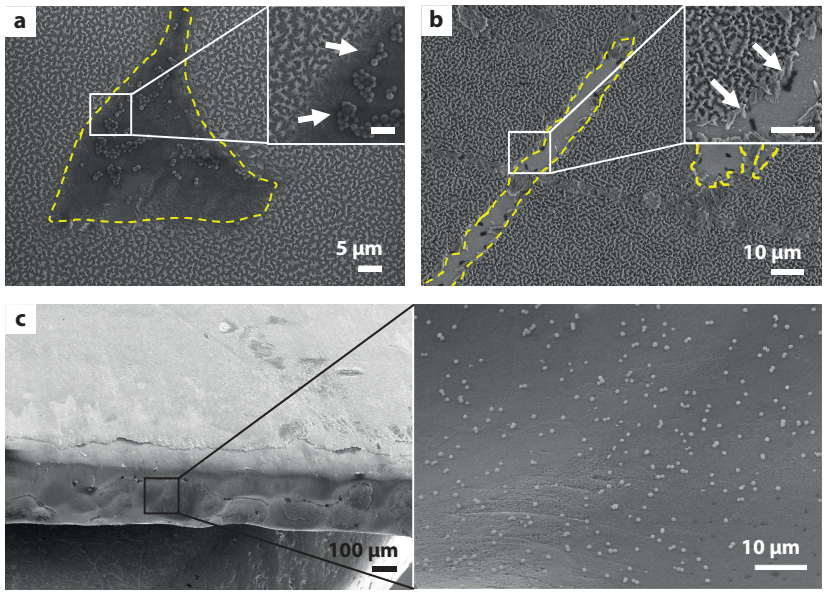

Figure 8. *FE-SEM images of bacterial adhesion on defective areas of hydrophobic nanopillared surfaces. (a) Edge area of the sample, showing no bacteria adhering on the hydrophobic nanopillared surface but adhering bacteria (S. aureus) on the flat sidewall without nanopillars. (b, c) S. aureus and E. coli adhering on damaged areas, respectively. Dashed lines in panels b and c indicate damaged areas. Each inset in (b) and (c) shows higher magnification of the damaged area, where arrows indicate the bacteria retained on the damaged area. The scale bar in each inset indicates 3 µm.*

Whereas the FE-SEM results (Figure 7) reveal hydrophobic nanopillared surfaces are virtually bacteria-free under flow, regardless of the bacterial strain, they do not directly agree with the noticeable numbers of CFUs measured by agar plating although the numbers on the hydrophobic nanopillared surfaces were significantly less than the other specimens (Figure 4). As shown in Figure 8, this is attributed to bacteria adhering on the sidewalls of the samples' edges where there is no effective nanostructure present and also on defective areas over the surfaces (especially boundary regions) that were inevitably caused during the sample handling (i.e. damage by tweezers). The flat sidewalls of the samples' edge (0.5 mm thick) provided a significant surface area, i.e., about 20 mm^2 (= 1 cm × 0.5 mm × 4), for bacterial adhesion (Figure 8a). The defective areas lost their 3D nanopillared surface morphology and therewith superhydrophobicity (i.e. air entrapment) and consequently acted as a flat surface that allowed the direct contact with the bacterial suspension and bacterial adhesion (Figure 8b and 8c). Figure 8 also clearly shows that the intact (undamaged) areas of the hydrophobic nanopillared surfaces are virtually bacteria-free, indicating that the noticeable CFUs found in the agar plating partly resulted from the bacteria retained on such defective areas. The results suggest that the superhydrophobically-engineered 3D nanopillared surfaces, with minimization of such defective or undefined areas with nanostructures, can provide the aluminum substrate with the extremely low bacterial adhesion capability.

CONCLUSIONS

Anodizing and post-etching followed by drying in air have enabled us to design and fabricate various types of nanostructured surfaces on aluminum substrates, including 2D nanoporous and 3D nanopillared surfaces. Spin-coating of a nanoscopically thin layer of Teflon has further allowed us to regulate the surface hydrophobicity without affecting the structural dimensions and integrity. Compared to an electropolished flat surface, the 2D nanoporous surfaces showed a significant reduction in CFU adhesion for *S. aureus* and *E. coli*, which was more pronounced for the hydrophobic surface condition. The 3D nanopillared surfaces showed an even larger reduction in CFU adhesion, also more pronounced for the hydrophobic surface condition resulting in slippery, superhydrophobicity. Shear due to fluid flow enhanced the reductions observed significantly, likely due to the influence of reduced contact areas between adhering bacteria and the nanostructured surfaces. Such fluid shear effect was more effective on the superhydrophobically-engineered 3D-nanopillared surface due to the effective entrapment of air layer on the surface which will result in the enhancement of the hydrodynamic detachment force. Such effects also appeared more dramatic in the case of *S. aureus* than *E. coli*, which is attributed to the spherical-shaped isotropic cell morphology of *S. aureus* as opposed to the rod-shaped anisotropic of *E. coli*. The anodizing and electrochemical etching techniques employed for aluminum substrates in this study are simple, scalable, and adaptable to various types of metallic materials so that the 3D nanopillared surfaces modulated with surface hydrophobicity would be of great significance in many antimicrobial applications such as in biomaterials implantology, water systems, and food processing, where biofilm formation is widespread public health problem.

Table 1. Prior works on the effect of micro/nanostructured surfaces on bacterial adhesion

Fabrication Method	Surface Pattern: Surface Material	Surface Pattern: Pattern Shape	Surface Pattern: Dimensions (λ, t, or d, h or R_a)	Surface Wettability	Surface Coating or Treatments	Bacteria Type (Gram-positive, Gram-negative)	Flow Condition	Main Results
Dip coating	Silica	Particles	d=220 nm – 1 µm	Hydrophilic, Hydrophobic, Super-hydrophobic	POTS for hydrophobicity	*E. coli* (-)	Static	Reduced bacterial adhesion up to 70% on hydrophobic paper and up to 99% on superhydrophobic paper.[18]
Soft lithography	Poly-urethane	Pillar	λ=800 nm – 5.5 µm, t=400 nm – 4 µm	Hydrophilic, Hydrophobic, Super-hydrophobic	Plasma cleaning for hydrophilicity	*S. epidermidis* (+)	Rotational shear	The submicron structured surfaces with increased hydrophobicity reduced bacterial adhesion by around 80%, while the micron patterned surfaces and hydrophilicity increased the adhesion.[19]
Plasma etching for Si	Teflon & Si	Pore	d=0.2-1 µm, λ=2-10 µm,	Hydrophilic, Hydrophobic, Super-hydrophobic	Oil coating for lubrication	*P. aeruginosa* (-), *S. aureus* (+), *E. coli* (-)	Flow	Oil-infused porous Teflon surfaces showed biofilm-free properties compared to superhydrophobic Si surfaces.[20]
E-beam patterning	PEG hydrogel	Pillar	λ=0.5-3.0 µm, t=400 nm, h=120 nm	Hydrophilic	NA	*S. aureus* (+)	Flow	About 85% reduced adhesion below 1.5 µm spacing distance.[21]
Plasma etching	SiO_2	Pillar	λ=200 nm, t=~50 nm, h=500 nm	Hydrophilic	NA	*P. aeruginosa* (-), *S. aureus* (+), *B. subtilis* (+)	Static	Nanopillars effectively killed bacteria (killing rate up to 450,000 bacteria/cm^2 per minute) .[22]
Laser interference lithography	Si	Pillar	λ=200-800 nm, t=75-300 nm, h=500 nm	Hydrophilic	NA	*S. epidermidis* (+), *S. aureus* (+)	Static & Flow	Reduced bacterial adhesion force with reduced contact area, resulting in easier detachment and higher transmission.[23]
Anodization	TiO_2	Tube	d=80 nm, h=400 nm	Hydrophilic	Gentamicin loading into nanotubes	*S. epidermis* (+)	Static	About 55% decreased adhesion on nanotubes filled with gentamicin compared to flat Ti and nanotubes without gentamicin.[24]
Anodization	TiO_2	Tube	d=20-80 nm	Hydrophilic	Heat treatment for crystallinity	*S. epidermidis* (+), *S. aureus* (+)	Static	About 25% reduced bacteria on especially 80 nm tubular.[25]

Table 1. continued

Fabrication Method	Surface Pattern: Surface Material	Surface Pattern: Pattern Shape	Surface Pattern: Dimensions (λ, t, or d, h or R_a)	Surface Wettability	Surface Coating or Treatments	Bacteria Type (Gram-positive, Gram-negative)	Flow Condition	Main Results
Anodization	TiO_2	Tube	d=80 nm, h=400 nm	Hydrophilic, Hydrophobic, Super-hydrophobic	PTES for hydrophobicity	*S. aureus* (+)	Static	About 85% reduced adhesion on flat hydrophobic Ti and more reduced (93%) on superhydrophobic nanotubular surfaces, compared to hydrophilic (uncoated) nanotubular surface.[26]
Anodization	TiO_2	Tube & Pillar	Pore: d=55 nm, h=1 µm; Pillar: λ=2 µm, h=2 µm	Hydrophilic	TA/G antimicrobial coating	*S. aureus* (+)	Flow	Increased antibacterial efficacy on nanopillared surfaces with 90% decrease in bacterial adhesion, compared to flat Ti.[27]
Grit - satin blasting, grinding	Ti alloy	Random roughness	R_a= 6 nm - 33 µm	Hydrophilic	NA	*S. epidermidis* (+)	Static	Both vertical and lateral roughness are important on bacterial adhesion; The bacterial adhesion was more on Satin (R_a= 0.83) and Grit-blasted (R_a= 11) compared to polished surface.[28]
Anodization	TiO_2	Tube	d=20-100 nm, h=110-300 nm	Hydrophilic	NA	*S. aureus* (+), *S. epidermidis* (+)	Static	About 25% reduced adhesion on nanoporous and nanotubular.[29]
Plasma coating	DLC & Fluoro-polymer	Random roughness	Stainless Steel: R_a=58-62 nm; DLC: 93-122 nm; AR: 33-248 nm	Hydrophilic, Hydrophobic	NA	*S. epidermidis* (+), *D. geothermalis* (+), *M. silvanus* (-), *Psx. Taiwanensis* (-)	Static	Diamond-like carbon (hydrophilic) and fluoropolymer (hydrophobic) surfaces decreased the adherence of all bacteria, 50 and 70%, respectively, compared to non-coated stainless steel surface.[30]
Anodization	**Al_2O_3**	**Pore & Pillar**	**Pore: d=28 nm, h=1.5 µm; Pillar: λ= 28 nm - 1 µm, h=1–1.5 µm**	**Hydrophilic, Hydrophobic, Super-hydrophobic**	**Teflon coating for hydrophobicity**	***S. aureus* (+), *E. coli* (-)**	**Static & Flow**	**More than 99% reduction in bacterial adhesion for both strains on superhydrophobic nanopillared surfaces under flow condition.**

λ, structural pitch; *t*, tip size (for line or pillar); *d*, diameter (for tube or pore); *h*, height or depth; R_a, surface arithmetic average roughness parameter; DDS, dimethyldich-lorosilane; POTS, 1*H*,1*H*,2*H*,2*H*-perfluorooctyltriethoxysilane; FAAO, fluoroalkylated acrylic acid oligomer; PTES, 1*H*, 1*H*, 2*H*, 2*H*-perfluorooctyl-triethoxysilane; NA, not applicable; TA/G, Tannic acid/Gentamicin; (+), Gram-positive; (-), Gram-negative; DLC, diamond-like carbon; AR, Alu-Releco Oy fluoropolymer

Supporting Information

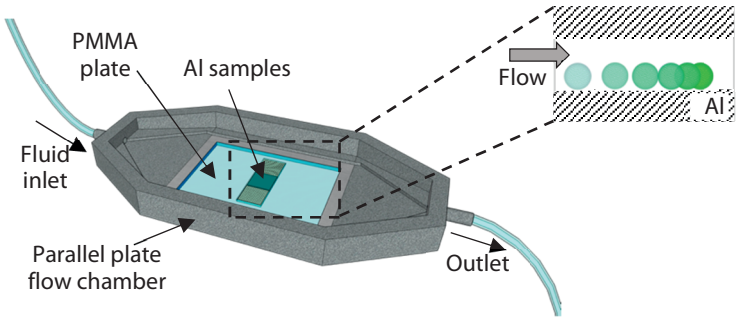

Figure S1. *Schematics of the parallel-plate flow chamber. A stainless steel flow chamber is used, with aluminum (Al) samples placed into 1 cm × 1 cm and 0.5 mm deep sockets to level out with the PMMA bottom plate of the chamber to suppress potential interference and turbulent flow at the edges of the samples. The locations of the flat, 2D nanoporous, and 3D nanopillared samples were interchanged at each of triplicated adhesion experiments to compensate for possible differences caused by the conditions of different locations on the bottom plate. Color change of bacteria indicates the flow in between the two parallel plates. Triplicated adhesion experiments were carried out with separately cultures bacteria.*

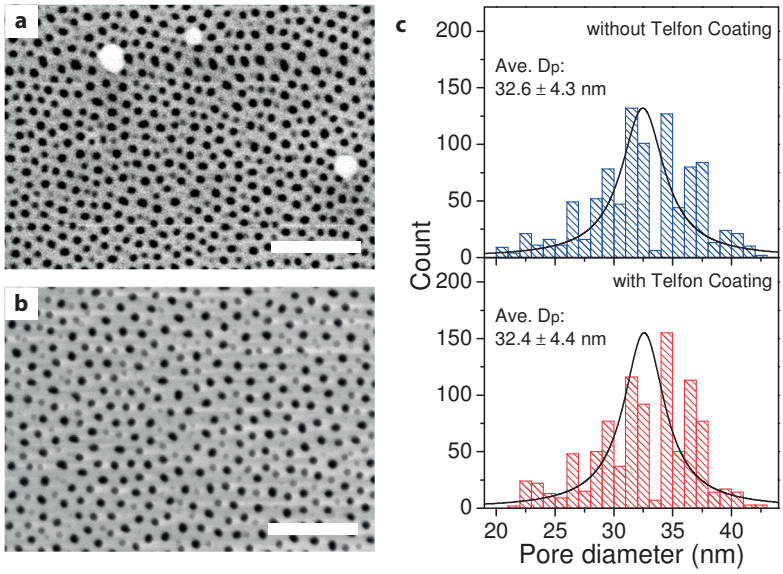

Figure S2. *(a-b) FE-SEM images of the nanoporous AAO layers before (a) and after (b) Teflon coating. Scale bars indicate 500 nm. (c) Distribution of the pore diameter estimated fro m the FE-SEM images of the nanoporous AAO layers before and after the Teflon coating, indicating that the Teflon coating thickness is not more than a couple of nanometers. For more precise image analysis, the nanopore structures were opened by post-etching for 15 min.*

REFERENCES

1. Lewin, R. Microbial Adhesion Is a Sticky Problem. *Science* 1984, *224*, 375–377.
2. McLean, R. J. C.; Nickel, J. C.; Olson, M. E. Biofilm Associated Urinary Tract Infections. In *Microbial biofilms*; Lappin-Scott, H. M.; Costerton, J. W., Eds.; Cambridge University Press: Cambridge, United Kingdom, 1995; pp. 261–273.
3. Kumar, C. G.; Anand, S. K. Significance of Microbial Biofilms in Food Industry: A Review. *Int. J. Food Microbiol.* 1998, *42*, 9–27.
4. Little, B.; Wagner, P.; Hart, K.; Ray, R.; Lavoie, D.; Nealson, K.; Aguilar, C. The Role of Biomineralization in Microbiologically Influenced Corrosion. *Biodegradation* 1998, *9*, 1–10.
5. Spellberg, B.; Bartlett, J. G.; Gilbert, D. N. The Future of Antibiotics and Resistance. *N. Engl. J. Med.* 2013, *368*, 297–299.
6. Klibanov, A. M. Permanently Microbicidal Materials Coatings. *J. Mater. Chem.* 2007, *17*, 2479–2482.
7. Mukherjee, K.; Rivera, J. J.; Klibanov, A. M. Practical Aspects of Hydrophobic Polycationic Bactericidal "paints". *Appl. Biochem. Biotechnol.* 2008, *151*, 61–70.
8. Tang, H.; Wang, A.; Liang, X.; Cao, T.; Salley, S. O.; McAllister, J. P.; Ng, K. Y. S. Effect of Surface Proteins on *Staphylococcus epidermidis* Adhesion and Colonization on Silicone. *Colloids Surf. B. Biointerfaces* 2006, *51*, 16–24.
9. Cao, Z.; Sun, Y. Polymeric N-Halamine Latex Emulsions for Use in Antimicrobial Paints. *ACS Appl. Mater. Interfaces* 2009, *1*, 494–504.
10. Kenawy, E.-R.; Worley, S. D.; Broughton, R. The Chemistry and Applications of Antimicrobial Polymers: A State-of-the-Art Review. *Biomacromolecules* 2007, *8*, 1359–1384.
11. Liu, Y.; He, T.; Gao, C. Surface Modification of Poly(ethylene Terephthalate) via Hydrolysis and Layer-by-Layer Assembly of Chitosan and Chondroitin Sulfate to Construct Cytocompatible Layer for Human Endothelial Cells. *Colloids Surf. B. Biointerfaces* 2005, *46*, 117–126.
12. Mao, Z.; Ma, L.; Gao, C.; Shen, J. Preformed Microcapsules for Loading and Sustained Release of Ciprofloxacin Hydrochloride. *J. Control. Release* 2005, *104*, 193–202.
13. Nejadnik, M. R.; Van der Mei, H. C.; Norde, W.; Busscher, H. J. Bacterial Adhesion and Growth on a Polymer Brush-Coating. *Biomaterials* 2008, *29*, 4117–4121.
14. Vogler, E. A. Structure and Reactivity of Water at Biomaterial Surfaces. *Adv. Colloid Interface Sci.* 1998, *74*, 69–117.
15. Bos, R.; Van der Mei, H. C.; Gold, J.; Busscher, H. J. Retention of Bacteria on a Substratum Surface with Micro-Patterned Hydrophobicity. *FEMS Microbiol. Lett.* 2000, *189*, 311–315.
16. Campoccia, D.; Montanaro, L.; Arciola, C. R. A Review of the Biomaterials Technologies for Infection-Resistant Surfaces. *Biomaterials* 2013, *34*, 8533–8554.
17. Decuzzi, P.; Ferrari, M. Modulating Cellular Adhesion through Nanotopography. *Biomaterials* 2010, *31*, 173–179.
18. Yang, H.; Deng, Y. Preparation and Physical Properties of Superhydrophobic Papers. *J. Colloid Interface Sci.* 2008, *325*, 588–593.
19. Xu, L.-C.; Siedlecki, C. A. *Staphylococcus Epidermidis* Adhesion on Hydrophobic and Hydrophilic Textured Biomaterial Surfaces. *Biomed. Mater.* 2014, *9*, 35003.
20. Epstein, A. K.; Wong, T.-S.; Belisle, R. A.; Boggs, E. M.; Aizenberg, J. Liquid-Infused Structured Surfaces with Exceptional Anti-Biofouling Performance. *Proc. Natl. Acad. Sci. U. S. A.* 2012, *109*, 13182–13187.
21. Wang, Y.; Subbiahdoss, G.; Swartjes, J.; Van der Mei, H. C.; Busscher, H. J.; Libera, M. Length-Scale Mediated Differential Adhesion of Mammalian Cells and Microbes. *Adv. Funct. Mater.* 2011, *21*, 3916–3923.
22. Ivanova, E. P.; Hasan, J.; Webb, H. K.; Gervinskas, G.; Juodkazis, S.; Truong, V. K.; Wu, A. H. F.; Lamb, R. N.; Baulin, V. A.; Watson,

G. S.; *et al.* Bactericidal Activity of Black Silicon. *Nat. Commun.* 2013, *4*, 2838.

23. Hizal, F.; Choi, C.-H.; Busscher, H. J.; Van der Mei, H. C. Staphylococcal Adhesion, Detachment and Transmission on Nanopillared Si Surfaces. *ACS Appl. Mater. Interfaces* 2016, *8*, 30430–30439.
24. Popat, K. C.; Eltgroth, M.; Latempa, T. J.; Grimes, C. A.; Desai, T. A. Decreased *Staphylococcus Epidermis* Adhesion and Increased Osteoblast Functionality on Antibiotic-Loaded Titania Nanotubes. *Biomaterials* 2007, *28*, 4880–4888.
25. Ercan, B.; Taylor, E.; Alpaslan, E.; Webster, T. J. Diameter of Titanium Nanotubes Influences Anti-Bacterial Efficacy. *Nanotechnol.* 2011, *22*, 295102.
26. Tang, P.; Zhang, W.; Wang, Y.; Zhang, B.; Wang, H.; Lin, C.; Zhang, L. Effect of Superhydrophobic Surface of Titanium on *Staphylococcus Aureus* Adhesion. *J. Nanomater.* 2011, *2011*, 178921.
27. Hizal, F.; Zhuk, I.; Sukhishvili, S.; Busscher, H. J.; Van der Mei, H. C.; Choi, C. H. Impact of 3D Hierarchical Nanostructures on the Antibacterial Efficacy of a Bacteria-Triggered Self-Defensive Antibiotic Coating. *ACS Appl. Mater. Interfaces* 2015, *7*, 20304–20313.
28. Wu, Y.; Zitelli, J. P.; TenHuisen, K. S.; Yu, X.; Libera, M. R. Differential Response of Staphylococci and Osteoblasts to Varying Titanium Surface Roughness. *Biomaterials* 2011, *32*, 951–960.
29. Pérez-Jorge, C.; Conde, A.; Arenas, M. A.; Pérez-Tanoira, R.; Matykina, E.; De Damborenea, J. J.; Gõmez-Barrena, E.; Esteban, J. In Vitro Assessment of *Staphylococcus Epidermidis* and *Staphylococcus Aureus* Adhesion on TiO_2 Nanotubes on Ti-6Al-4V Alloy. *J. Biomed. Mater. Res. - Part A* 2012, *100 A*, 1696–1705.
30. Raulio, M.; Järn, M.; Ahola, J.; Peltonen, J.; Rosenholm, J. B.; Tervakangas, S.; Kolehmainen, J.; Ruokolainen, T.; Narko, P.; Salkinoja-Salonen, M. Microbe Repelling Coated Stainless Steel Analysed by Field Emission Scanning Electron Microscopy and Physicochemical Methods. *J. Ind. Microbiol. Biotechnol.* 2008, *35*, 751–760.
31. Muszanska, A. K.; Nejadnik, M. R.; Chen, Y.; Van den Heuvel, E. R.; Busscher, H. J.; Van der Mei, H. C.; Norde, W. Bacterial Adhesion Forces with Substratum Surfaces and the Susceptibility of Biofilms to Antibiotics. *Antimicrob. Agents Chemother.* 2012, *56*, 4961–4964.
32. Jeong, C.; Choi, C.-H. Single-Step Direct Fabrication of Pillar-on-Pore Hybrid Nanostructures in Anodizing Aluminum for Superior Superhydrophobic Efficiency. *ACS Appl. Mater. Interfaces* 2012, *4*, 842–848.
33. Scallan, E.; Hoekstra, R. M.; Angulo, F. J.; Tauxe, R. V.; Widdowson, M. A.; Roy, S. L.; Jones, J. L.; Griffin, P. M. Foodborne Illness Acquired in the United States-Major Pathogens. *Emerg. Infect. Dis.* 2011, *17*, 7–15.
34. Fan, J. G.; Dyer, D.; Zhang, G.; Zhao, Y. P. Nanocarpet Effect: Pattern Formation during the Wetting of Vertically Aligned Nanorod Arrays. *Nano Lett.* 2004, *4*, 2133–2138.
35. Zhao, Y. P.; Fan, J. G. Clusters of Bundled Nanorods in Nanocarpet Effect. *Appl. Phys. Lett.* 2006, *88*, 1–4.
36. Zhao, Q.; Liu, Y.; Wang, C.; Wang, S.; Peng, N.; Jeynes, C. Reduction of Bacterial Adhesion on Ion-Implanted Stainless Steel Surfaces. *Med. Eng. Phys.* 2008, *30*, 341–349.
37. Hutter, J. L.; Bechhoefer, J. Calibration of Atomic-Force Microscope Tips. *Rev. Sci. Instrum.* 1993, *64*, 1868.
38. Masuda, H.; Hasegwa, F.; Ono, S. Self-Ordering of Cell Arrangement of Anodic Porous Alumina Formed in Sulfuric Acid Solution. *J. Electrochem. Soc.* 1997, *144*, L127.
39. Li, A. P.; Müller, F.; Birner, A.; Nielsch, K.; Gösele, U. Hexagonal Pore Arrays with a 50–420 Nm Interpore Distance Formed by Self-Organization in Anodic Alumina. *J. Appl. Phys.* 1998, *84*, 6023.
40. Wenzel, R. N. Resistance of Solid Surfaces to Wetting by Water. *Ind. Eng. Chem.* 1936, *28*, 988–994.
41. Lee, J.; Shin, S.; Jiang, Y.; Jeong, C.; Stone, H. A.; Choi, C.-H. Oil-Impregnated Nanoporous Oxide Layer for Corrosion Protection with

Self-Healing. *Adv. Funct. Mater.* 2017.

42. Cassie, A. B. D.; Baxter, S. Wettability of Porous Surfaces. *Trans. Faraday Soc.* 1944, *40*, 546.
43. Autumn, K.; Sitti, M.; Liang, Y. A.; Peattie, A. M.; Hansen, W. R.; Sponberg, S.; Kenny, T. W.; Fearing, R.; Israelachvili, J. N.; Full, R. J. Evidence for Van Der Waals Adhesion in Gecko Setae. *Proc. Natl. Acad. Sci. U. S. A.* 2002, *99*, 12252–12256.
44. Nejadnik, M. R.; Van der Mei, H. C.; Busscher, H. J.; Norde, W. Determination of the Shear Force at the Balance between Bacterial Attachment and Detachment in Weak-Adherence Systems, Using a Flow Displacement Chamber. *Appl. Environ. Microbiol.* 2008, *74*, 916–919.
45. Lee, C.; Choi, C. H.; Kim, C. J. Superhydrophobic Drag Reduction in Laminar Flows: A Critical Review. *Exp. Fluids* 2016, *57*, 176.
46. Luong-Van, E.; Rodriguez, I.; Low, H. Y.; Elmouelhi, N.; Lowenhaupt, B.; Natarajan, S.; Lim, C. T.; Prajapati, R.; Vyakarnam, M.; Cooper, K. Review: Micro- and Nanostructured Surface Engineering for Biomedical Applications. *J. Mater. Res.* 2013, *28*, 165–174.
47. Svensson, S.; Forsberg, M.; Hulander, M.; Vazirisani, F.; Palmquist, A.; Lausmaa, J.; Thomsen, P.; Trobos, M. Role of Nanostructured Gold Surfaces on Monocyte Activation and *Staphylococcus Epidermidis* Biofilm Formation. *Int. J. Nanomedicine* 2014, *9*, 775–794.